The Mechanism of the Freshwater Outflow Through the Ganges - Brahmaputra - Meghna Delta

Kida, Shinichiro
Research Institute for Applied Mechanics, Kyushu University

Yamazaki, Dai
Institute of Industrial Science, The University of Tokyo

出版情報：Water Resources Research. 56 (6), pp.e2019WR026412-, 2020-06. American Geophysical Union
バージョン：
権利関係：Creative Commons Attribution 4.0 International

Water Resources Research

RESEARCH ARTICLE
10.1029/2019WR026412

Special Section:
Coastal hydrology and oceanography

The Mechanism of the Freshwater Outflow Through the Ganges-Brahmaputra-Meghna Delta

Shinichiro Kida[1] and Dai Yamazaki[2]

[1]Research Institute for Applied Mechanics, Kyushu University, Kasuga, Japan, [2]Institute of Industrial Science, The University of Tokyo, Tokyo, Japan

Key Points:
- The dynamics of river discharge through the Ganges-Brahmaputra-Meghna delta to the Bay of Bengal were investigated using a two-layer model
- Active river-ocean interactions occur within the distributaries due to sea surface perturbation induced by a river plume
- Increased river outflow at the main stem can cause backwater at the mouths of the distributaries, inducing upstream flow

Supporting Information:
- Supporting Information S1

Correspondence to:
S. Kida,
kida@riam.kyushu-u.ac.jp

Citation:
Kida, S., & Yamazaki, D. (2020). The mechanism of the freshwater outflow through the Ganges-Brahmaputra-Meghna delta. *Water Resources Research*, *56*, e2019WR026412. https://doi.org/10.1029/2019WR026412

Received 26 SEP 2019
Accepted 28 APR 2020
Accepted article online 4 MAY 2020

Abstract The Ganges-Brahmaputra-Meghna (GBM) delta is a major source of freshwater for the Bay of Bengal. The flow through this megadelta is complex because of its large size and numerous river networks, making the region a challenging area for river-routing models. This study investigates the dynamics of the riverine outflow across the GBM delta and its interaction with the ocean on monthly to seasonal time scales, using a two-layer model that represents the riverine water and the oceanic water. The model simulates a seasonal increase and decrease of discharge and sea surface height (SSH) at both the main stem and the distributaries. Although discharge through the main stem is driven by that propagating from the upstream, model experiments show that the distributaries are an active region of river-ocean interactions as a result of a river plume established on the oceanic side of the river mouth. This river plume is induced by river discharge in the presence of the Coriolis force and is associated with an increase in SSH along the coast. Backwater is induced at the river mouth, resulting in convergence and higher SSH in distributaries. The narrow, meandering, and shallow paths of the distributaries enhance the role of friction on the flow from the upstream, making their river mouths more sensitive to oceanic variability. The results of our study demonstrate that river plumes may play a central role in the dynamics of megadelta flow by connecting the dynamics at the main stem and the distributaries with ocean dynamics.

1. The Ganges-Brahmaputra-Meghna Delta

The Ganges-Brahmaputra-Meghna (GBM) delta is a megadelta that stretches hundreds of kilometers along the coast of the Bay of Bengal (Figure 1); it is the largest delta worldwide, comprising numerous freshwater and sediment plumes that flow into to the ocean. Freshwater entering from the GBM delta is a major source of low-salinity water at the surface of the Bay of Bengal (Akhil et al., 2014; Behara & Vinayachandran, 2016; Han & McCreary, 2001).

Because the GBM delta is barely above sea level, frequent flooding makes this region vulnerable to climate variability. Riverine and coastal flooding are anticipated to increase due to climate change (Hirabayashi et al., 2013; Karim & Mimura, 2008). River discharge is driven by the Indian Monsoon, which develops during the boreal summer, with a maximum discharge of about 82,000 $m^3\ s^{-1}$ in August–September, a minimum of less than 10,000 $m^3\ s^{-1}$ in late winter (Papa et al., 2012), and an annual average of about 32,000 $m^3\ s^{-1}$ (Dai & Trenberth, 2002). Oceanic processes such as tides and storm surge cause backwater and coastal flooding by perturbing the sea surface height (SSH) near the river mouth. Numerical models have shown that these signals penetrate the GBM delta toward inland; controlling factors include bathymetry, channel width, river discharge, and bed friction (Bricheno et al., 2016; Karim & Mimura, 2008). Storm surges can occasionally lead to compound events, such that riverine and coastal flooding occur simultaneously, and affect a region as much as 200 km inland (Ikeuchi et al., 2017; Lewis et al., 2013).

Because the GBM delta supports the activities of a large population and serves as an important source of surface freshwater for the Bay of Bengal, it is important to understand how flows through its various distributary channels are controlled. However, observations and simulations of flows through this megadelta are difficult due to its extensive size and complexity of the river network. The single downstream assumption and kinematic wave approach adopted by many traditional large-scale hydrodynamic models are incapable of simulating flows through a river network involving multiple bifurcations and confluences. Proper treatment of bifurcation is necessary for realistically simulating floods and river discharge over a large area (Ikeuchi et al., 2015, 2017; Neal et al., 2012; Yamazaki et al., 2014). At a delta, riverine water interacts

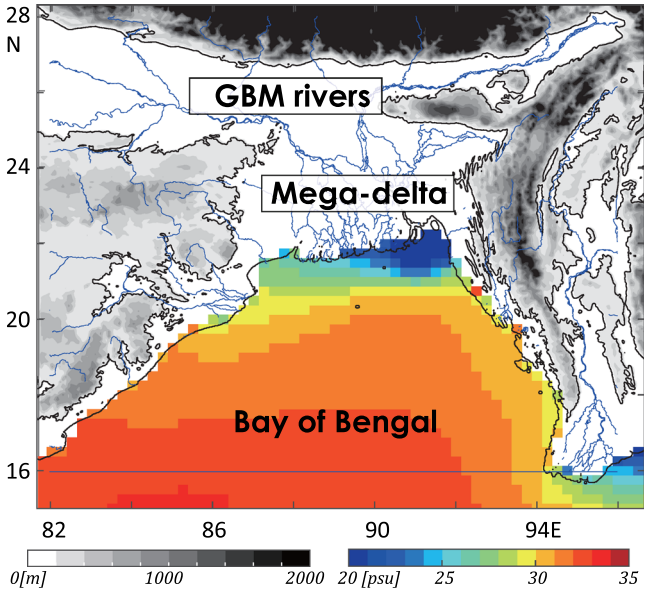

Figure 1. Annual mean surface salinity of the Bay of Bengal (color) and the Ganges-Brahmaputra-Meghna (GBM) (solid blue lines) river network. Salinity is based on Soil Moisture Active Passive (SMAP) from 2015 to 2018 (Meissner et al., 2018). The river network is based on Global Self-consistent, Hierarchical, High-resolution Geography Database (GSHHG) (Wessel & Smith, 1996). Gray shading shows bathymetry on land, where black solid lines are the coastlines and 200 m above sea level.

with the oceanic water (Figure 2a). Past studies of river-ocean interactions have mainly focused on the impacts of tides and storm surges, which occur on time scales of a few hours to a few days (Bricheno et al., 2016; Ikeuchi et al., 2017). How river-ocean interactions occur at longer time scales, such as the monthly to seasonal time scales of monsoon-driven events, remains unknown. Satellite observations show the monsoonal winds, local and remote, inducing Kelvin waves that perturb the SSH along the coast of Bay of Bengal. An annual cycle is observed with a drop in SSH from January to April and a rise from May to August and October to November (Rao et al., 2010). The SSH changes are about 0.3 m on a monthly average, which is about half of that observed near the river mouths of the GBM delta (Figure 3c). A river-routing model that incorporates the impact of sea level changes along the coast by coupling it to an oceanic model also simulates a seasonal SSH signal at the GBM delta (Ikeuchi et al., 2017). Oceanic changes are not always external to the delta system; river discharge can also induce oceanic changes that may, in turn, affect river discharge in a feedback process.

When riverine water reaches the ocean, geostrophic adjustment due to Earth's rotation forces the bulk of riverine water to turn to the right (in the Northern Hemisphere), resulting in a coastal current that increases SSH along the coast. This feature is known as a river plume (Figure 2b; see Horner-Devine et al. 2015 for a thorough review). Because river plumes can travel along the coast over much longer distances than the spatial scale of a river mouth, they can propagate to other river mouths, where they may alter the river discharge. Observations have shown river plumes changing coastline SSH at the continental scale (e.g., Piecuch et al., 2018). Past theoretical studies of river plumes have primarily focused on single-channel river; however, multiple river channels, such as those in a delta, can interact through the formation of a river plume in the ocean. In the GBM delta, the river plume with the largest transport is likely that created by the main stem; the rivers most greatly affected by this river plume are likely the distributaries (Figure 2b). Hydrological models often assume that the dynamics at each river mouth are independent and therefore neglect oceanic processes that connect the dynamics between river mouths. Oceanic models, on the other hand, often prescribe river discharges for each river mouth and neglect oceanic processes that alter this discharge. These approaches may be reasonable for single-channel rivers, but not for a megadelta.

How does the GBM riverine water enter the Bay of Bengal through the megadelta? Will the dynamics of the GBM delta differ to those of a single-channel river? Does the formation of river plumes matter? In the present study, we focus on the role of river plumes on a megadelta by using a two-layer model representing riverine water and oceanic water and investigate the impact of river-ocean interaction behind the GBM river discharge. Section 2 describes the model setup and the experiments in detail. Section 3 presents model results from experiments using realistic topography and compares these results to observations. The dynamics along the distributary are further examined through experiments using idealized topography in section 4. A summary and discussion are provided in section 5.

2. Model Experiments and Observations

2.1. The GBM Delta Model

A two-layer model of the GBM delta is created using the Hallberg Isopycnal Model (HIM), with the upper (lighter) layer representing the riverine freshwater and the lower (denser) layer representing the oceanic water (Figure 2a). The technical details of the model are provided in Hallberg and Rhines (1996**)** and Hallberg (1997). This two-layer setup allows explicit representation of freshwater and oceanic water, unlike one-layer hydrodynamic models, which cannot distinguish the two water masses. The basic governing equations for the freshwater layer are as follows:

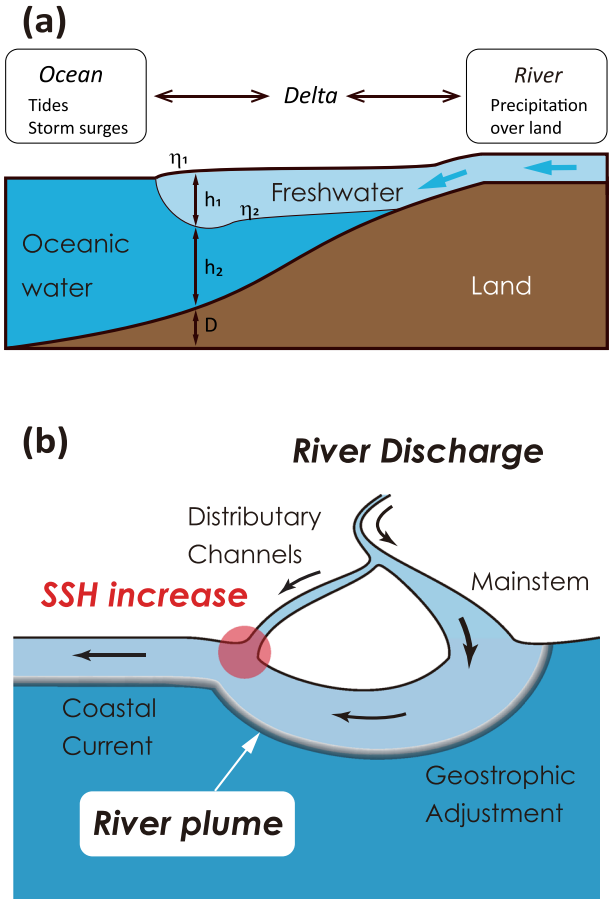

Figure 2. (a) Vertical cross section of the freshwater and oceanic layers across a delta and possible external forces that may induce variability in river discharge. (b) Plan view of the river plume induced at the river mouth of the main stem and its influence on the distributary channels.

$$\frac{\mathrm{d}\boldsymbol{u_1}}{\mathrm{d}t}+f\hat{\boldsymbol{k}}\times\boldsymbol{u_1}=-g\nabla\eta_1+K_H\nabla^2\boldsymbol{u_1}-\frac{\boldsymbol{\tau_{int}}}{h_1} \quad (1)$$

$$\frac{\partial h_1}{\partial t}+\nabla\cdot(\boldsymbol{u_1}h_1)=w^*-\alpha h_1 \quad (2)$$

and those for the oceanic layer are as follows:

$$\frac{\mathrm{d}\boldsymbol{u_2}}{\mathrm{d}t}+f\hat{\boldsymbol{k}}\times\boldsymbol{u_2}=-g\nabla\eta_1-g'\nabla\eta_2+K_H\nabla^2\boldsymbol{u_2}+\frac{\boldsymbol{\tau_{int}}}{h_2}-C_D\frac{U}{h_2}\boldsymbol{u_2} \quad (3)$$

$$\frac{\partial h_2}{\partial t}+\nabla\cdot(\boldsymbol{u_2}h_2)=-w^* \quad (4)$$

where subscripts 1 and 2 represent the freshwater and oceanic layers, respectively; $\boldsymbol{u}$ is the horizontal flow; f is the Coriolis parameter, where $f = 6 \times 10^{-5}$ s^{-1} for the study region; and $\hat{\boldsymbol{k}}$ is the unit vertical vector. The reduced gravity is represented by $g' = (\rho_2 - \rho_1)g/\rho_1$, where ρ_1 is 1,000 kg m^{-3} and ρ_2 is 1,030 kg m^{-3}. Wind stress is absent, and the interfacial stress $\boldsymbol{\tau_{int}}$ is $\frac{2K_Z(u_1-u_2)}{h_1+h_2}$. SSH is represented by $\eta_1 = h_1+h_2+D$, and the interface height is represented by $\eta_2 = h_2+D$, where D is the bottom bathymetry and h is the thickness. The entrainment velocity from the lower layer to the upper layer is represented by w^*, which is estimated based on the Richardson number following Turner (1986), and α is the restoring parameter. The lateral and vertical viscosity coefficients K_H and K_Z are set to 1.65 and 1×10^{-4} m^2 s^{-1}, respectively, which is similar to past modeling studies on river plumes (e.g., Cole & Hetland, 2016; Iwanaka & Isobe, 2018). Model results are not overly sensitive to K_H. Quadratic bottom drag is represented by the drag coefficient C_D (=0.001) and flow speed U, which is estimated by the vertical average of the flow in the bottom 10 m. This setup follows the basic configuration of HIM and is identical to that used in Kida and Yamashiki (2015).

Two-layer models have been used extensively for oceanic studies (e.g., Cushman-Roisin & Beckers, 2011). We adopted this modeling approach instead of coupling a river model and an ocean model at the river mouth for two reasons. First, the two-layer model expresses the movement of freshwater and oceanic water explicitly. Second, it captures the interaction between the river and ocean at the river mouth seamlessly because the model setup does not differ between water sources. HIM can handle zero layer thickness; therefore, it does not include a dry/wet scheme, and flows and layer thicknesses are determined by solving equations 1–4.

The model domain covers 20.5–23.75°N and 86.5–92.5°E with a horizontal resolution of about 550 m (Figure 3a). The land surface elevation is based on the SRTM3 DEM (Farr et al., 2007) with hydrological adjustment following the HydroSHEDS flowlines (Yamazaki et al., 2012). The hydrological adjustment is performed at 3-arcsec resolution (about 90 m), and then the elevation data are upscaled to a 550 m resolution by taking the minimum value so that the connectivity of small channels and distributaries is represented. The channel bathymetry is based on topography parameter sets used in the global discharge model CaMa-Flood (Yamazaki et al., 2014). To ensure that narrow river pathways are connected, areas with elevation between 0 and 2 m are considered to represent rivers and are deepened to −1 m. Bathymetry below sea level is considered to represent ocean, and GEBCO2014 (Weatherall et al., 2015) is used with a minimum depth of −5 m. Depressed areas within the delta deeper than −5 m are modified to −5 m. The maximum open ocean depth is −50 m. To focus on the flow field through the GBM delta near the main stem, bathymetry is simplified far from the main stem (west of 89°E and east of 92°E); oceanic bathymetry on the eastern side of the main stem is kept realistic to avoid unnecessary influence on the river plume since it is located on the upstream side of the delta, where a river plume is expected to develop.

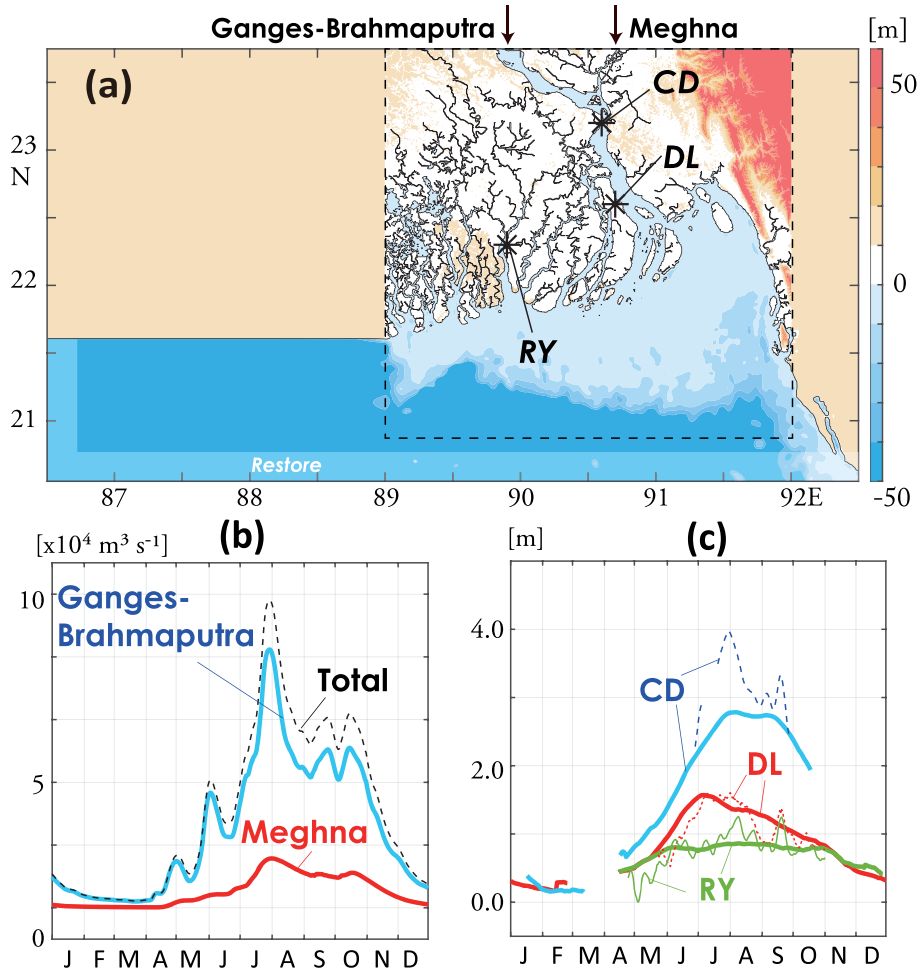

Figure 3. (a) Bathymetry of the REXP experiment. River inflows for the GBM delta are prescribed at the northern boundary. Black solid lines are the coastlines. Asterisks indicate the locations of the Chandpur (CD), Daulatkhan (DL), and Rayenda (RY) tidal gauge stations. The freshwater layer is restored along the western and southern boundaries. (b) Daily discharge of the Ganges-Brahmaputra River (thick blue line) and the Meghna River (thick red line), and the total discharge (thin dashed black line) for 2004 acquired from CaMa-Flood (Yamazaki et al., 2014). (c) The 7-day running average of sea surface height (SSH) observed at CD (thin dashed blue line), DL (thin dotted red line), and RY (thin solid green line) in 2004. SSH is offset using the minimum value observed during 2000–2010. Climatological values for 2000–2010 are shown as thick solid lines.

Initially, oceanic water is present from the bottom to 0 m and the freshwater layer is absent. Freshwater is introduced at the northern boundary on Day 1 based on the daily discharge of the Ganges-Brahmaputra and Meghna Rivers as simulated by CaMa-Flood (Yamazaki et al., 2014) and integrated for 1 year. Simulated daily discharge resembles the observed discharge (Ikeuchi et al., 2017; Papa et al., 2012). We used outputs from 2004, when a large flooding event occurred in the region (Figures 3b and 3c). The northern boundary of the main stem is about 4 m below sea level and about 200 km inland; therefore, we expected river-ocean interaction to be small. The lateral boundaries are closed, and the freshwater layer thickness is restored to 0 within about 30 km near the western and southern boundaries at $\alpha = 1\ \mathrm{day}^{-1}$. This makes the freshwater layer gradually disappear and avoids the accumulation of freshwater within the model domain. Hereafter, we refer to the experiment based on these settings above as REXP.

The model realistically simulates the seasonal discharge through the GBM delta (Figure 4b). To further examine the role of oceanic processes on the flow field, we performed two sensitivity experiments: NOCF examines the role of the Coriolis force by setting the Coriolis parameter to 0; WALL examines the role of the ocean by inserting a wall to disconnect the flow field of the main stem river mouths from those of the distributaries.

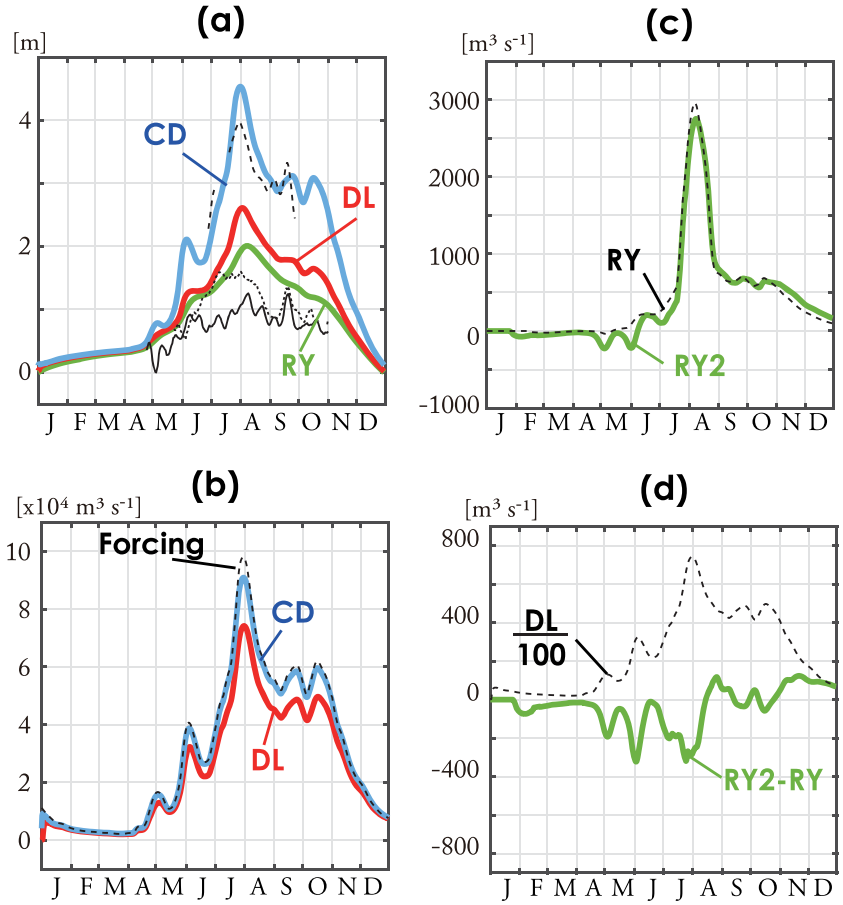

Figure 4. Time series of REXP. (a) SSH at CD (thick blue line), DL (thick red line), and RY (thick green line). SSH observed at CD (thin dashed black line), DL (thin dotted black line), and RY (thin solid black line) in 2004 (as in Figure 3c). (b) Discharge at CD (blue line) and DL (red line) and total discharge forced (dashed black line). (c) Discharge at RY (dashed black line) and RY2 (thick green line). (d) Discharge at DL (dashed black line) and the difference between RY and RY2 (RY2 − RY; thick green line). Note that the discharge for DL is shown as 1% of the actual magnitude.

2.2. Observed SSH (Water Level)

SSH observations obtained from tidal gauge stations at Chandpur, Daulatkhan, and Rayenda are used to compare the model simulations to observations (Figure 3a; Ikeuchi et al., 2017). Although the term "water level" is frequently used to express the height of the river water surface, we will use SSH because the focus of our study is more on river mouths. Chandpur (upstream) and Daulatkhan (downstream) are located along the main stem. Rayenda is located on one of the distributaries and is about 50 km upstream of the river mouth.

Climatological SSH is estimated using observations collected from 2000 to 2010 with a 30-day running average, excluding missing values (Figure 3c). The absolute SSH is unknown; therefore, the minimum value observed at each location is used as the zero reference level. This minimum appears to occur in early spring when the discharge is lowest. Rayenda observations lacked data from winter to spring; therefore, SSH at this location is offset using values observed in late spring, which could lead to a bias toward lower values. The climatological peak observed in Chandpur at the end of June, which occurs a month earlier than the peak upstream, could be related to the role of the monsoonal winds and the propagation of the Kelvin waves along the coast of Bay of Bengal from spring to summer (Rao et al., 2010). Observed SSH at Chandpur in 2004 shows a large peak in late July, which is captured by CaMa-Flood (Figure 3b). Weekly variation is more recognizable at Rayenda, perhaps due to local precipitation, intrinsic ocean variability, or tides.

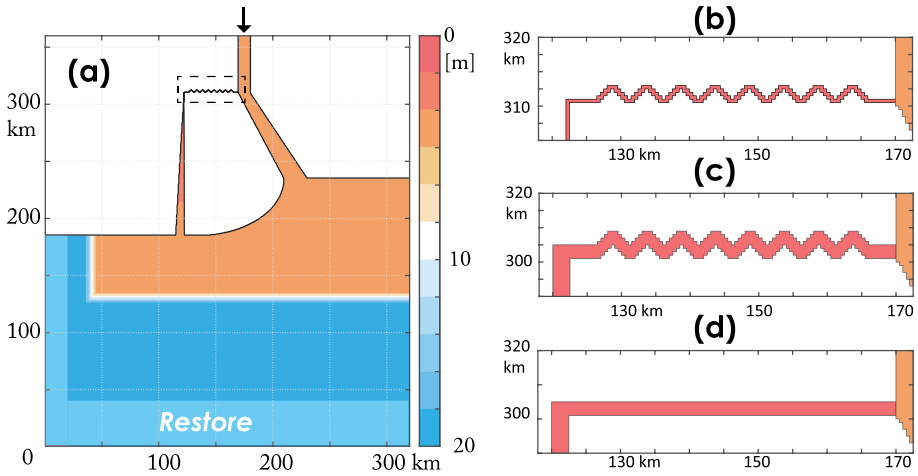

Figure 5. *Figure*(a) Bathymetry of the IDLZ experiment. River inflow is prescribed at the northern boundary, and the freshwater layer is restored along the western and southern boundaries. Close-ups of the region bounded by the black-dashed box are shown for the (b) CTRL, (c) WIDE, and (d) STRT experiments.

2.3. Idealized River Delta Model

The dynamics behind the river-ocean interaction is further examined by simplifying the REXP bathymetrical setting (Figure 3a) for a delta consisting of a main stem and a single distributary (Figure 5a); this experiment is hereafter referred to as IDLZ. The main stem is 5 km wide at upstream, becoming wider toward the river mouth. The depth is 5 m within the shelf and deepened offshore to a maximum of 50 m. The distributary is 225 km long and is narrow (500 m) and shallow (1 m) in the meandering upstream zonal segment (Figure 5b); in the meridional segment, the width and depth increase linearly toward the river mouth to 3.5 km and 5 m, respectively.

Freshwater is introduced at the northern boundary with a sinusoidally varying discharge as follows:

$$V=\frac{V_o}{2}\left[1-\cos\left(\frac{2\pi t}{60}\right)\right], \tag{5}$$

where $V_o=2\times10^4$ m^3 s^{-1} and t is time (days). The magnitude and variability of this discharge represent the short-term variation that occurs around early June (Figure 3b). The model is integrated for 180 days. All other conditions for IDLZ are the same as those for REXP, including the restoration of the freshwater thickness to 0 along the western and southern boundaries of the model domain.

To explore the sensitivity of the dynamics of flow along the distributary, three experiments are conducted. WIDE examines the impact of the narrow width of the distributary by increasing the river width in the zonal segment in IDLZ to 2 km while maintaining the remaining bathymetric conditions (Figure 5c). STRT examines the impact of sinuosity by removing the meanders in WIDE (Figure 5d). DEEP examines the impact of the river depth by setting the depth of the distributary channel in STRT to 5 m, that is, the depth of the main stem. All three experiments are identical to IDLZ except for the distributary bathymetrical settings.

3. Model Results

After a few months, the model results show GBM riverine freshwater entering the ocean through various channels and establishing a river plume along the coast to cover the entire megadelta (Figure 6). The freshwater layer is trapped along the coast and flows geostrophically toward the west, which is characteristic of a river plume. The thickness and transport of this river plume increase or decrease following the changes in the river discharge.

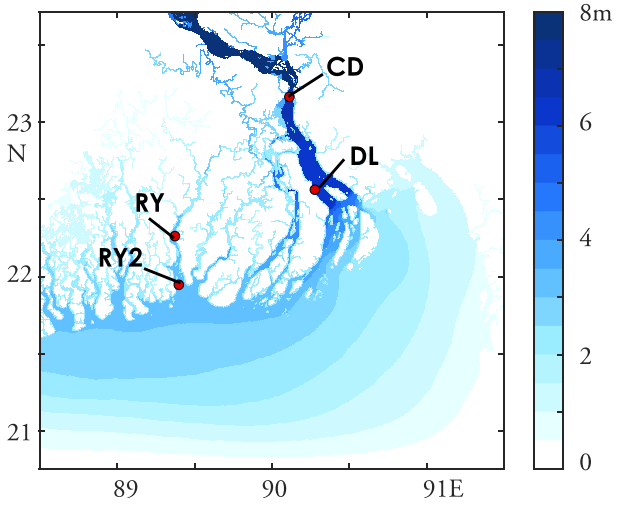

Figure 6. Thickness of the freshwater layer on Day 180 for the REXP experiment within the dashed box region shown in Figure 3a. Red circles are the locations of CD, DL, RY, and 25 km downstream of Rayenda (RY2).

3.1. Flow Through the Main Stem

In the main stem, the seasonal SSH cycle simulated for Chandpur reflects the seasonal cycle of river discharge forcing at the northern boundary (Figures 3a and 3b). The magnitude of the seasonal SSH cycle at Chandpur is about 3 m, which matches well with observations. A minimum occurs from winter to spring, and a maximum occurs from late summer to early fall. SSH at Chandpur also shows a sharp increase and decrease in late July, which match well with observations (Figure 3c). For Daulatkhan, the magnitude of the seasonal cycle is about 2 m. Compared to Chandpur, the seasonal cycle at Daulatkhan is nearly 1.5 m lower from spring to fall. This decrease in SSH likely occurs because the river width is wider at Daulatkhan than at Chandpur and to support the downstream flow via a pressure gradient. The increase and decrease of SSH at Daulatkhan occur at similar months as Chandpur but are larger than observations by about 1.0 m after summer and lacks the peak in June. The simulated SSH at Daulatkhan shows a sharp peak in late July, which appears to be absent from the observations, perhaps due to the flooding event that occurred following the strong river discharge peak in July 2004 (Islam et al., 2010); flooding typically results in part of the riverine water escaping to land. The river width and depth used in our model may have been too great to allow such flooding events to be simulated. The overestimate may also originate from forced river discharge; however, this possibility cannot explain why simulated SSH shows a peak that matches observations at Chandpur but not at Daulatkhan. We also find some sensitivity to the model domain size which will be discussed in the next subsection.

The seasonal cycle of discharge at Chandpur matches the total discharge forced from the northern boundary (Figure 4b). However, the discharge at Daulatkhan is lower than that at Chandpur, despite its downstream position. This result may be explained by part of the flow entering distributaries between Chandpur and Daulatkhan. The discharge at Daulatkhan is about 85% of that at Chandpur, such that the remaining 15% enters the distributaries. It is unclear whether this ratio is realistic due to lack of observations, but it is similar to values reported in a previous modeling study (Haque & Rahman, 2016). Our model results show that the ratio entering the distributary slightly decreases when discharge is low but remains roughly constant year-round.

3.2. Flow Through a Distributary

The simulated SSH at Rayenda shows an increase and decrease following the simulated seasonal discharge cycle at the main stem (Figure 4a). A maximum occurs in late July, and a minimum occurs in winter. The magnitude of the seasonal cycle is about 1.5 m, which is about 0.5 m larger compared to observations after summer. Part of this large value may originate from the location of the southern boundary in the model (supporting information Figure S1). The distance from the river mouth is about the size of the barotropic deformation radius (about 165 km), and a weaker SSH signal is simulated in summer at Rayenda and Daulatkhan when the southern boundary is moved further south. However, the basic behavior of the flow near the river mouths remains largely unaffected because river plumes and river-ocean interaction occur within the baroclinic deformation radius scale (about 30 km) from the river mouth. Uncertainty also exists in the absolute observation height due to the lack of data from winter to spring, as mentioned in section 2.2, and in the bathymetry of the distributary channels in the model, in which we chose to use a depth of −1 m to connect the river lines. However, we find the SSH to change by only a few centimeters when a shallower depth is used. A higher-resolution model and bathymetric data are needed for further examination of the impacts of river depth and width. The largest differences are found in late July, when a sharp increase and decrease are observed in the main stem, possibly related to the flood event as mentioned above for the seasonal cycle at Daulatkhan. Simulated SSH at Rayenda is smoother than the observations, with variability absent at a weekly time scale (Figures 3c and 4a), likely due to a lack of variability from forcing (Figure 3b) or winds, tides, and local precipitation events, which are not included in our model.

The discharge simulated at Rayenda is more than one order smaller than that of the main stem (Figures 4b and 4c). The accumulation of these small distributaries creates a 15% reduction in the main stem discharge from Chandpur to Daulatkhan. The seasonal discharge cycle shows a slow increase from spring to early summer, but an abrupt increase occurs at the end of July. This trend differs from the seasonal cycle observed for SSH, where a linear increase is detected from spring to early summer. The difference between discharge and SSH is not observed at Daulatkhan, where discharge increases as SSH increases (Figure 4a). Therefore, this difference suggests that another process is responsible for the increases and decreases in discharge through a distributary, in addition to the propagation of flow from the upstream. If the increase and decrease in SSH at Rayenda occur solely due to flow propagating from the upstream, its trend should more closely resemble that of the discharge.

Discharge at a location 25 km downstream from Rayenda is characterized by flow in the upstream direction in late spring (i.e., negative discharge in Figure 4c). The cause for this flow reversal near the river mouth is likely the river plume that forms in the ocean. Differences in discharge from that at Rayenda (negative = lower discharge downstream) show variability on a monthly time scale, identical to that observed at Daulatkhan but in the opposite phase (Figure 4d). Because discharge at Rayenda does not show variability on a monthly time scale, the variability must originate from the oceanic side, and the negative difference in late spring indicates backwater and convergence in the distributary (Figure 6). Model results indicate that river plumes affect the flow inside distributaries through SSH perturbation in distributaries west of the main stem (Figure 2b). In our model, distributaries that are not directly connected to the main stem have no background riverine water coming from the upstream so flows at these distributaries show variability that is forced solely by the river plume; an upstream and downstream flow is induced following the enhancement or reduction of the river plume.

3.3. Coriolis Force and Oceanic Effects

The formation of a river plume requires the presence of the Coriolis force and a long coast. The Coriolis force allows geostrophic adjustment that makes riverine freshwater flow along constant SSH (roughly equivalent to pressure contours). In the absence of the Coriolis force, flow is down the SSH gradient (or pressure gradient), resulting in a downstream decrease in SSH. A long coast allows freshwater to propagate, possibly affecting SSH at other river mouths. Therefore, we test the importance of a river plume in REXP by setting the Coriolis parameter to 0 (NOCF) or isolating the river mouths of the distributaries from the main stem using a wall (WALL).

In NOCF, the SSH at Rayenda shows a seasonal cycle similar to that of REXP but with one half of the magnitude (Figure 7d). This reduction in SSH is detected across the delta and ocean, especially to the west of the main stem (Figure 7b), confirming the presence of geostrophic balance in increasing the SSH toward the right side of the flow (looking downstream) and the SSH at Rayenda in REXP. A meridional decrease in SSH occurs in NOCF because SSH gradient is required to support the meridional flow from land to the ocean. The importance of the Coriolis force for the SSH increase at Rayenda is dynamically consistent with the fact that the increase in SSH across the distributary makes pressure gradient weak throughout the region and induces weak flow compared to the main stem. Otherwise, a large SSH gradient would emerge between the main stem and the distributary, resulting in an unrealistically strong flow.

In WALL, the SSH at Rayenda decreases significantly compared with that of REXP (Figures 7c and 7d). The amount of freshwater near the river mouths of the distributary located west of the main stem is much smaller because the propagation of the river plume is blocked by a wall. The increase in SSH in the distributaries must occur solely by propagation from upstream; however, this signal appears slowly and cannot increase SSH at Rayenda from spring to summer, as observed upstream in the main stem. Variability is noticeable at the monthly time scale from late spring to early summer in REXP and NOCF and is absent in WALL (Figure 7d). The model results from NOCF and WALL strongly indicate that the river plume induced by the main stem plays a crucial role in the dynamics governing the seasonal flow cycles through distributaries.

4. The River-Ocean Interaction in the Distributaries

4.1. The Idealized Model

Next, we use IDLZ to further examine the mechanism behind the river-ocean interaction within the distributary (Figures 5a and 5b). As shown in section 2, IDLZ has simple bathymetrical conditions and river

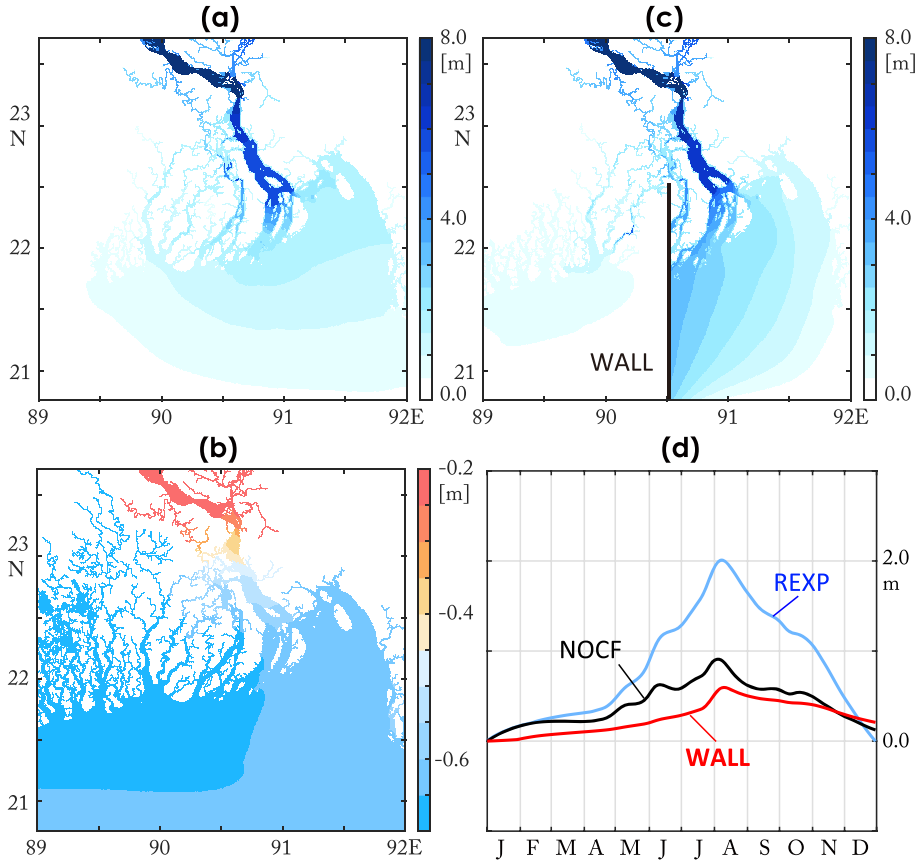

Figure 7. (a) Freshwater thickness on Day 180 for the NOCF experiment. (b) The difference in SSH between NOCF and REXP (NOCF − REXP). (c) Freshwater thickness on Day 180 for the WALL experiment. (d) Time series of SSH at Rayenda for the REXP (blue line), NOCF (black line), and WALL (red line) experiments.

discharge forced at the main stem resembling that of the GBM river discharge during spring (equation 5). The model results show the formation of a river plume along the coast and upstream flow near the river mouth of the distributary when the discharge of the main stem increases (Figures 8a and 8b); this flow field is similar to that found in REXP.

The flow field within the distributary shows that flows near the upstream bifurcation point change as the flow in the main stem changes (Figure 8c). SSH along the distributary also shows this signal propagating slowly downstream (Figure 8d). In contrast, flows near the river mouth are changing roughly in the opposite phase of that in the main stem, because flows near the river mouth are induced by the river plume that perturbs SSH near the river mouth. SSH along the distributary shows this signal propagating quickly in the upstream direction (Figure 8d). When SSH at the river mouth is slightly higher than in the interior of the distributary, flow is forced upstream. The upstream propagation speed based on the tilt of the SSH is about 2.3 m s^{-1}, which is about twice the baroclinic gravity wave speed ($\sqrt{g'h}$=1.2 m s^{-1}). The difference likely reflects the increase in SSH by the flow from the upstream, which creates additional convergence and a rise in the SSH within the distributary. Changes in SSH in the interior of the distributary show that convergence or divergence between the flows forced at the river mouth and the upstream are responsible for the increase or decrease in SSH within the distributary (Figures 8c and 8d).

4.2. The Roles of River Width, Sinuosity, and Depth

The flow near the river mouth of the distributary is more greatly affected by the river plume in the ocean than by the flow from the upstream; the distance from the bifurcation point to the river mouth is shorter

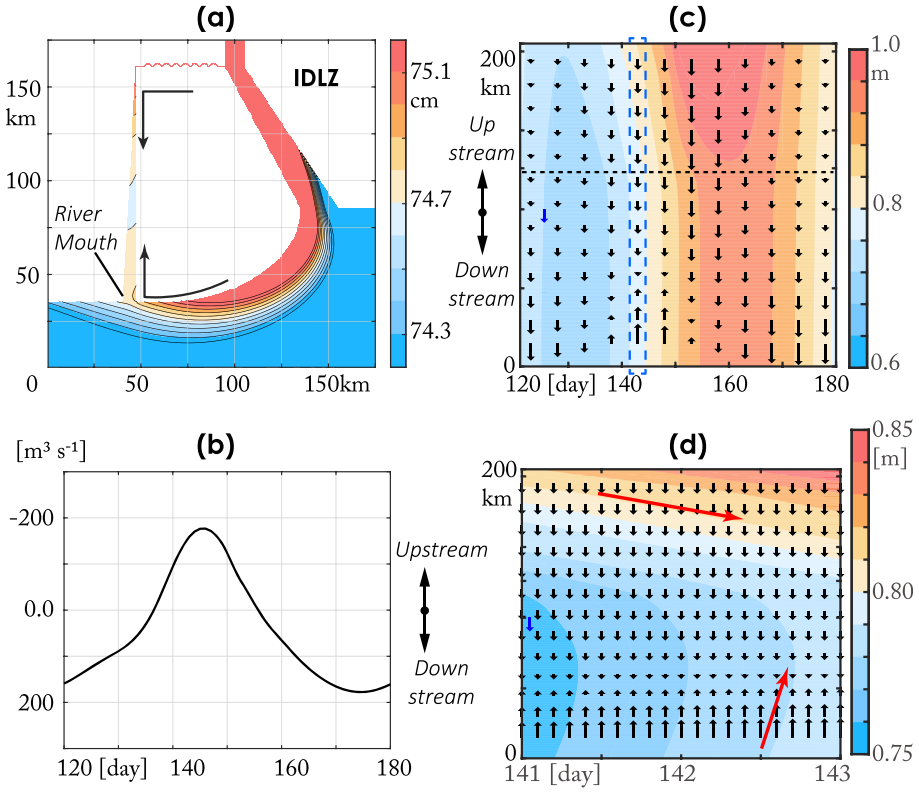

Figure 8. (a) Snapshot of SSH on Day 140 for the IDLZ experiment within the dotted square box in Figure 5a. (b) River discharge at the distributary 10 km from the river mouth between Days 120 and 180 for IDLZ. (c) SSH and discharge along the distributary for IDLZ. Distance is from the river mouth (0 km) to the upstream end of the zonal channel (210 km). Dashed line indicates where the distributary turns zonal. The blue vector shows a river discharge of 100 m^3/s. (d) A close-up of SSH and discharge within the blue dashed box in (c). The blue vector shows a river discharge of 100 m^3/s.

along the distributary than along the main stem and coast; therefore, perturbation signals are likely to reach the river mouth through the distributary first in the absence of friction. We next examine the effects of the narrow, meandering, and shallow aspects of the distributary on river-ocean interactions occurring at the river mouth in three experiments: WIDE, STRT, and DEEP (Figures 5c and 5d).

In WIDE, stagnant flow occurs in the distributary near the river mouth when the main stem flow increases (Figures 9a and 9b). A decrease in the flow occurs like IDLZ; however, the impact of the river plume on the distributary is reduced. In STRT, the impact of the river plume on the distributary is even smaller, and the flow through the distributary is now downstream throughout the forcing period (Figure 9b and 9c). These experiments show that the narrow and meandering features of the distributary partly explain why the flow near the river mouth responds to the river plume.

The roles of the narrow and meandering features are clarified by diagnosing the zonal momentum balance in the zonal segment of the distributary. We first derive this equation from equation 1 by taking an area integral over the zonal segment of the distributary (Figure10a), such that equation 1 becomes

$$\iint \frac{d\boldsymbol{u_1}}{dt}\,dA + \iint f\hat{\boldsymbol{k}} \times \boldsymbol{u_1}\,dA = -\oint_C g\eta\hat{\boldsymbol{n}}\,ds + \iint K_H \nabla^2 \boldsymbol{u_1}\,dA - \iint \frac{\boldsymbol{\tau_{int}}}{h_1}\,dA. \tag{6}$$

where A is the area of the integration; the divergence theorem is used for the pressure gradient term, where C is the boundary of A and $\hat{\boldsymbol{n}}$ is its normal vector (McCabe et al., 2006). When focusing on the zonal momentum balance, the pressure gradient term can be partitioned into a sum of pressure drag due to the meandering wall and a pressure difference across the zonal boundaries of the distributary:

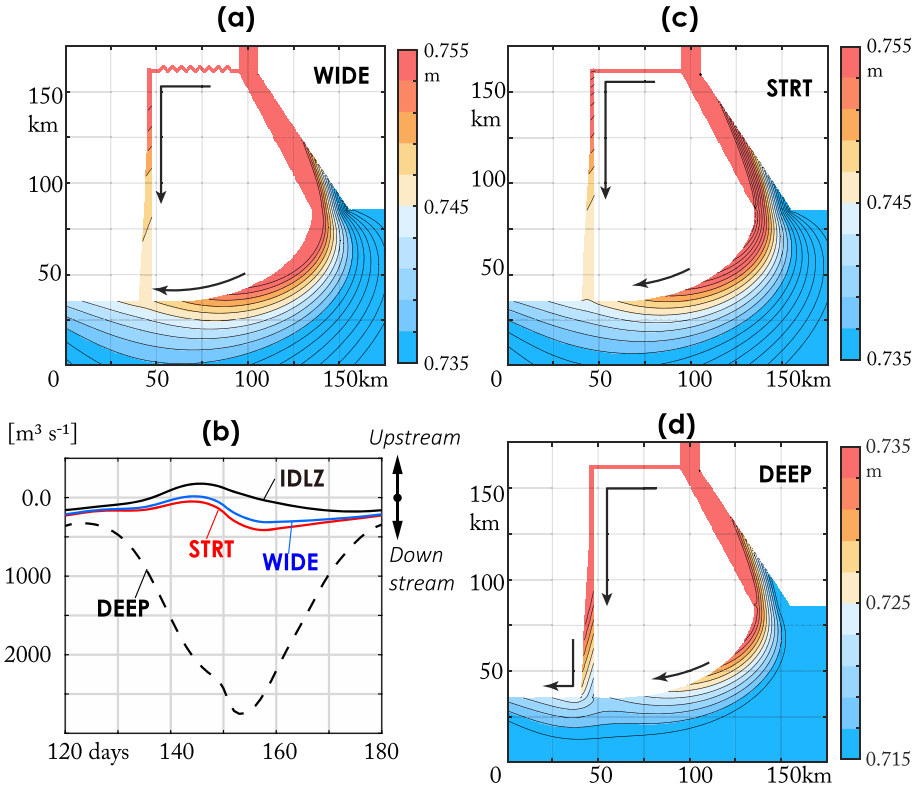

Figure 9. (a) Snapshot of SSH on Day 140 for the WIDE experiment within the dotted square box in Figure 5a. (b) River discharge at the distributary 10 km from the river mouth between Days 120 and 180 for IDLZ (black solid line), WIDE (blue line), STRT (red line), and DEEP (black dashed line). (c) Snapshot of SSH on Day 140 for the STRT and (d) DEEP experiments.

$$\text{Pressure drag}=\int_{x=X_W}^{x=X_E} g\eta_1(Y_N)\frac{\mathrm{d}Y_N}{\mathrm{d}x}\,\mathrm{d}s-\int_{x=X_W}^{x=X_E} g\eta_1(Y_S)\frac{\mathrm{d}Y_N}{\mathrm{d}x}\,\mathrm{d}s \tag{7}$$

and

$$\text{Pressure difference}=-gL(\eta_1(X_E)-\eta_1(X_W)). \tag{8}$$

The zonal and meridional axes are x and y, respectively, where Y_N, Y_S, X_W (=126.5 km), and X_E (=165.5 km) are the northern, southern, western, and eastern boundaries of the area integral, respectively (Figure 10a). L is the meridional length of the channel at X_W and X_E. The time average during Days 120–180 indicates that the terms on the left-hand side (LHS) of equation 6 are negligible compared to those on the right-hand side (RHS). Therefore, the zonal momentum balance along a distributary can be expressed as a balance between the pressure difference and a sum of pressure drag, lateral friction, and vertical friction:

$$gL[\eta_1(X_E)-\eta_1(X_W)]=\left[\int_{x=X_W}^{x=X_E} g\eta_1(Y_N)\frac{\mathrm{d}Y_N}{\mathrm{d}x}\,\mathrm{d}s-\int_{x=X_W}^{x=X_E} g\eta_1(Y_S)\frac{\mathrm{d}Y_N}{\mathrm{d}x}\,\mathrm{d}s\right]+\iint K_H\nabla^2 u_1\,\mathrm{d}A-\iint\frac{\tau_{int}}{h_1}\mathrm{d}A. \tag{9}$$

In IDLZ, the magnitudes of the pressure difference, pressure drag, lateral friction, and vertical friction per area are 1.47, 0.68, 0.14, and 0.64 m s^{-2}, respectively (Figure 10b). The pressure difference along the distributary is balanced by vertical friction and pressure drag, indicating that the role of friction is enhanced

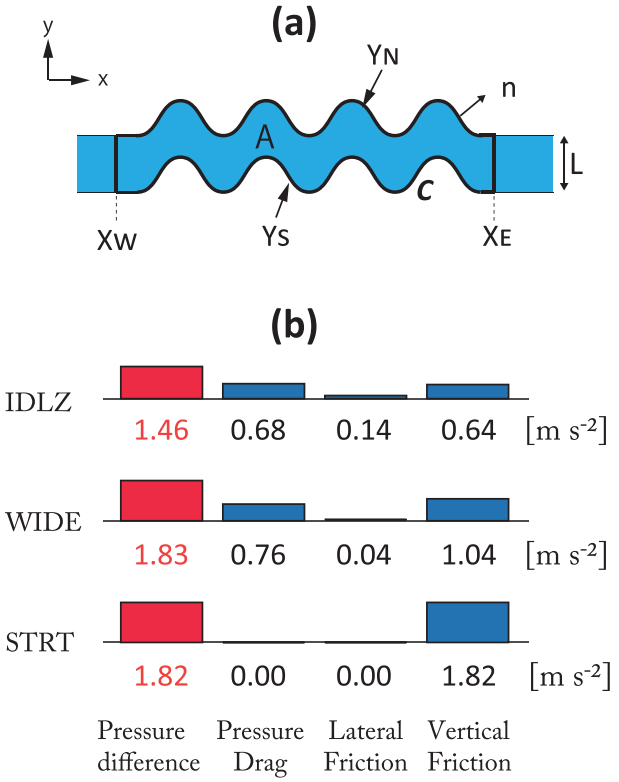

Figure 10. (a) Schematic of the zonal segment along the distributary and the parameters used for the area integral for equation 6. (b) The momentum balance along the distributary for IDLZ, WIDE, and STRT, per area. The term on the LHS of equation 9 is in red, and the terms on the RHS are in blue.

in meanders. In WIDE, the magnitudes of the pressure difference, pressure drag, lateral friction, and vertical friction per area are 1.83, 0.76, 0.04, and 1.04 m s^{-2}, respectively. Vertical friction plays a larger role than pressure drag as the channel width increases. The increased magnitude of the pressure gradient also reflects the increase in flow through the distributary, suggesting that the overall impact of friction is lower for a wider channel. In STRT, the magnitudes of the pressure difference, pressure drag, lateral friction, and vertical friction per area are 1.82, 0.00, 0.00, and 1.82 m s^{-2}, respectively. In the absence of meander, pressure drag is 0 by definition, such that the pressure difference is balanced by vertical friction.

In DEEP, strong flow in the downstream direction is found throughout the forcing period and the impact of the river plume is negligible (Figure 9b). As the channel deepens, the impact of vertical friction is significantly reduced from STRT, and the flow through the distributary becomes an order larger, with the increase and decrease in discharge now occurring in phase with those at the main stem (Figure 9b**)**. The model results show that in the absence of narrow, meandering, and shallow features in the distributary, river-ocean interactions do not occur along the distributary. Enhanced friction along the distributary reduces the flow and variability of water propagating downstream, allowing the oceanic feature to affect the flow in the distributary near the river mouth.

5. Summary and Discussion

5.1. Summary

The main goal of this study was to understand how riverine water enters the ocean through a megadelta. We focused on the GBM delta, the largest delta worldwide, and examined the role of the ocean on the river discharge at monthly to seasonal time scales. We hypothesized that distributary flows are affected by a river plume that establishes along the coast, making these distributaries an active region of river-ocean interactions.

We used a two-layer model representing riverine and oceanic water to simulate the seasonal cycle of the river discharge to examine the dynamics behind the river-ocean interactions. We found that about 85% of riverine water entered the Bay of Bengal through the main stem and this discharge from the main stem established a river plume that propagated westward along the coast. Coriolis force and the oceanic connection between the river mouths of the main stem and the distributaries were found capable of affecting the seasonal cycle of the flow field within the distributaries. Idealized model experiments showed that when a distributary was narrow, meandering, and shallow, the impact of friction was enhanced, weakening the propagation of flow in the downstream direction. As a result, perturbation signals propagating through the main stem and along the coast became the major drivers of variability at the river mouth of the distributaries. Backwater occurred at the river mouths of the distributaries and induced flow in the upstream direction that varied in the opposite phase as that of the main stem. Our findings indicate that river plumes, which are an oceanic response to river discharge, may play a central role in the dynamics of river outflow across a delta.

5.2. Discussion

Our model results suggest that two-layer models are useful for understanding the dynamics between rivers and the ocean across a delta. The application of conventional hydrodynamic models remains challenging for megadeltas, and the inclusion of river-ocean interaction may be a key process for their further improvement. Ikeuchi et al. (2017) showed that a realistic flow through the GBM delta at the main stem could be simulated by a state-of-the-art river-routing model which is coupled to an ocean model at the river mouth. However, the increase in the SSH observed from spring to summer remained weak at Rayenda, along the distributary (see Figure 3b in Ikeuchi et al., 2017). This may be partly because the coupling was one way, from the ocean

to rivers, which is the assumption often made in many river-routing models. The assumption makes the dynamics at the river mouths of the main stem and distributaries independent. However, as our model experiments show, additional SSH increase may also occur at the river mouths of the distributaries through an oceanic response to river discharge from the main stem. The inclusion of such a process in river-routing models would require a parameterization of the impact of river plumes that would connect the dynamics between river mouths.

Since we decided to keep our model as simple as possible, we neglected various features that are present at deltas, such as oceanic stratification and density changes to the riverine water and external processes, such as winds, oceanic circulation, and tides. Understanding the effects of these processes is the next step for this work. Winds can induce Kelvin waves that can raise the SSH near river mouths (Rao et al., 2010), but their spatial scale is large and will likely affect both the main stem and distributary flows simultaneously. Oceanic flows can alter the direction of a river plume and the region of active river-ocean interaction. Tides can create stronger velocity shear and enhance entrainment. Preliminary model experiments suggest that river-ocean interaction will nonetheless occur although the phase of the discharge may differ. River-ocean interaction may be more sensitive to enhanced vertical viscosity induced by tides. While vertical viscosity coefficient is likely to vary strongly in space and in time, we find that an increase of vertical viscosity uniformly by an order makes the river plume viscous and weakens the establishment of a river plume along the coast. The impact of river plumes on the distributaries is then reduced. As the spatial resolution of river-routing models and ocean models improves, there is a need to couple these models for more realistic simulations and to understand the impact of the ocean on rivers, and vice versa. Our findings suggest that active river-ocean interactions may occur through river plumes at other megadeltas worldwide. With the Coriolis force a crucial factor for river plume development, river-ocean interactions may become more active in river deltas at middle to high latitudes and weaker in river deltas near the equator.

Acknowledgments

The authors thank Dr. Hirabayashi for providing tidal gauge data for the GBM delta, Dr. Yosuke Yamashiki for discussion, and the two reviewers for their valuable comments. This work was supported by JSPS KAKENHI Grant JP16K17808. SMAP data were downloaded from the Asia-Pacific Data Research Center of the University of Hawaii at Manoa website (http://apdrc.soest.hawaii.edu). HIM was downloaded from Geophysical Fluid Dynamics Laboratory website (https://nomads.gfdl.noaa.gov/nomads/forms/him_beta_nomads.html).

References

Akhil, V. P., Durand, F., Lengaigne, M., Vialard, J., Keerthi, M. G., Gopalakrishna, V. V., et al. (2014). A modeling study of the processes of surface salinity seasonal cycle in the Bay of Bengal. *Journal of Geophysical Research: Oceans*, *119*, 3926–3947. https://doi.org/10.1002/2013JC009632

Behara, A., & Vinayachandran, P. N. (2016). An OGCM study of the impact of rain and river water forcing on the Bay of Bengal. *Journal of Geophysical Research: Oceans*, *121*, 2425–2446. https://doi.org/10.1002/2015JC011325

Bricheno, L. M., Wolf, J., & Islam, S. (2016). Tidal intrusion within a mega delta: An unstructured grid modelling approach. *Estuarine, Coastal and Shelf Science*, *182*, 12–26. https://doi.org/10.1016/j.ecss.2016.09.014

Cole, K. L., & Hetland, R. D. (2016). The effects of rotation and river discharge on net mixing in small-mouth kelvin number plumes. *Journal of Physical Oceanography*, *46*(5), 1421–1436. https://doi.org/10.1175/JPO-D-13-0271.1

Cushman-Roisin, B., & Beckers, J. M. (2011). *Introduction to geophysical fluid dynamics: Physical and numerical aspects (Vol. 101)*, Waltham, MA: Academic Press.

Dai, A., & Trenberth, K. E. (2002). Estimates of freshwater discharge from continents: Latitudinal and seasonal variations. *Journal of Hydrometeorology*, *3*(6), 660–687. https://doi.org/10.1175/1525-7541(2002)003<0660:EOFDFC>2.0.CO;2

Farr, T. G., Rosen, P. A., Caro, E., Crippen, R., Duren, R., Hensley, S., et al. (2007). The shuttle radar topography mission. *Reviews of Geophysics*, *45*, RG2004. https://doi.org/10.1029/2005RG000183

Hallberg, R. (1997). Stable split time stepping schemes for large-scale ocean modeling. *Journal of Computational Physics*, *135*(1), 54–65. https://doi.org/10.1006/jcph.1997.5734

Hallberg, R., & Rhines, P. (1996). Buoyancy-driven circulation in an ocean basin with isopycnals intersecting the sloping boundary. *Journal of Physical Oceanography*, *26*(6), 913–940. https://doi.org/10.1175/1520-0485(1996)026<0913:BDCIAO>2.0.CO;2

Han, W., & McCreary, J. P. Jr. (2001). Modeling salinity distributions in the Indian Ocean. *Journal of Geophysical Research*, *106*(C1), 859–877. https://doi.org/10.1029/2000JC000316

Haque, A., & Rahman, M. (2016). Flow distribution and sediment transport mechanism in the estuarine systems of Ganges-Brahmaputra-Meghna delta. *International Journal of Environmental Science and Development*, *7*(1), 22–30. https://doi.org/10.7763/IJESD.2016.V7.735

Hirabayashi, Y., Mahendran, R., Koirala, S., Konoshima, L., Yamazaki, D., Watanabe, S., et al. (2013). Global flood risk under climate change. *Nature Climate Change*, *3*(9), 816–821. https://doi.org/10.1038/nclimate1911

Horner-Devine, A. R., Hetland, R. D., & MacDonald, D. G. (2015). Mixing and transport in coastal river plumes. *Annual Review of Fluid Mechanics*, *47*(1), 569–594. https://doi.org/10.1146/annurev-fluid-010313-141408

Ikeuchi, H., Hirabayashi, Y., Yamazaki, D., Kiguchi, M., Koirala, S., Nagano, T., et al. (2015). Modeling complex flow dynamics of fluvial floods exacerbated by sea level rise in the Ganges–Brahmaputra–Meghna Delta. *Environmental Research Letters*, *10*(12), 124,011. https://doi.org/10.1088/1748-9326/10/12/124011

Ikeuchi, H., Hirabayashi, Y., Yamazaki, D., Muis, S., Ward, P. J., Winsemius, H. C., et al. (2017). Compound simulation of fluvial floods and storm surges in a global coupled river-coast flood model: Model development and its application to 2007 Cyclone Sidr in Bangladesh. *Journal of Advances in Modeling Earth Systems*, *9*(4), 1847–1862. https://doi.org/10.1002/2017MS000943

Islam, A. S., Haque, A., & Bala, S. K. (2010). Hydrologic characteristics of floods in Ganges-Brahmaputra-Meghna (GBM) delta. *Natural Hazards*, *54*(3), 797–811. https://doi.org/10.1007/s11069-010-9504-y

Iwanaka, Y., & Isobe, A. (2018). Tidally induced instability processes suppressing river plume spread in a nonrotating and nonhydrostatic regime. *Journal of Geophysical Research: Oceans*, *123*, 3545–3562. https://doi.org/10.1029/2017JC013495

Karim, M. F., & Mimura, N. (2008). Impacts of climate change and sea-level rise on cyclonic storm surge floods in Bangladesh. *Global Environmental Change*, *18*(3), 490–500. https://doi.org/10.1016/j.gloenvcha.2008.05.002

Kida, S., & Yamashiki, Y. A. (2015). A layered model approach for simulating high river discharge events from land to the ocean. *Journal of Oceanography*, *71*(1), 125–132. https://doi.org/10.1007/s10872-014-0254-4

Lewis, M., Bates, P., Horsburgh, K., Neal, J., & Schumann, G. (2013). A storm surge inundation model of the northern Bay of Bengal using publicly available data. *Quarterly Journal of the Royal Meteorological Society*, *139*(671), 358–369. https://doi.org/10.1002/qj.2040

McCabe, R. M., MacCready, P., & Pawlak, G. (2006). Form drag due to flow separation at a headland. *Journal of Physical Oceanography*, *36*(11), 2136–2152. https://doi.org/10.1175/JPO2966.1

Meissner, T., Wentz, F. J., & Manaster, A. (2018). Remote sensing systems SMAP ocean surface salinities [level 3 running 8-day], version 3.0 validated release. Remote sensing systems, Santa Rosa, CA, USA. Available online at www.remss.com/missions/smap, https://doi.org/10.5067/SMP30-3SPCS

Neal, J., Schumann, G., & Bates, P. (2012). A subgrid channel model for simulating river hydraulics and floodplain inundation over large and data sparse areas. *Water Resources Research*, *48*, W11506. https://doi.org/10.1029/2012WR012514

Papa, F., Bala, S. K., Pandey, R. K., Durand, F., Gopalakrishna, V. V., Rahman, A., & Rossow, W. B. (2012). Ganga-Brahmaputra river discharge from Jason-2 radar altimetry: An update to the long-term satellite-derived estimates of continental freshwater forcing flux into the Bay of Bengal. *Journal of Geophysical Research*, *117*, C11021. https://doi.org/10.1029/2012JC008158

Piecuch, C. G., Bittermann, K., Kemp, A. C., Ponte, R. M., Little, C. M., Engelhart, S. E., & Lentz, S. J. (2018). River-discharge effects on United States Atlantic and Gulf coast sea-level changes. *Proceedings of the National Academy of Sciences*, *115*(30), 7729–7734. https://doi.org/10.1073/pnas.1805428115

Rao, R. R., Kumar, M. G., Ravichandran, M., Rao, A. R., Gopalakrishna, V. V., & Thadathil, P. (2010). Interannual variability of Kelvin wave propagation in the wave guides of the equatorial Indian Ocean, the coastal Bay of Bengal and the southeastern Arabian Sea during 1993–2006. *Deep Sea Research Part I: Oceanographic Research Papers*, *57*(1), 1–13. https://doi.org/10.1016/j.dsr.2009.10.008

Turner, J. S. (1986). Turbulent entrainment: The development of the entrainment assumption, and its application to geophysical flows. *Journal of Fluid Mechanics*, *173*(431), 431–471. https://doi.org/10.1017/S0022112086001222

Weatherall, P., Marks, K. M., Jakobsson, M., Schmitt, T., Tani, S., Arndt, J. E., et al. (2015). A new digital bathymetric model of the world's oceans. *Earth and Space Science*, *2*(8), 331–345. https://doi.org/10.1002/2015EA000107

Wessel, P., & Smith, W. H. (1996). A global, self-consistent, hierarchical, high-resolution shoreline database. *Journal of Geophysical Research*, *101*(B4), 8741–8743. https://doi.org/10.1029/96JB00104

Yamazaki, D., Baugh, C. A., Bates, P. D., Kanae, S., Alsdorf, D. E., & Oki, T. (2012). Adjustment of a spaceborne DEM for use in floodplain hydrodynamic modeling. *Journal of Hydrology*, *436*, 81–91.

Yamazaki, D., Sato, T., Kanae, S., Hirabayashi, Y., & Bates, P. D. (2014). Regional flood dynamics in a bifurcating mega delta simulated in a global river model. *Geophysical Research Letters*, *41*, 3127–3135. https://doi.org/10.1002/2014GL059744